Research in Astronomy and Astrophysics, 25:025009 (13pp), 2025 February

https://doi.org/10.1088/1674-4527/ada422
CSTR: 32081.14.RAA.ada422

A Combined Smoothing Method of Ensemble Pulsar Timescale and Application for Pulsar Atomic Clock Combined Timescale

Tinggao Yang[1,2], Minglei Tong[1,2,3], Bian Li[1,2,3], Zhehao Zhang[1,2,3], Xingzhi Zhu[1,2], and Yuping Gao[1,2,3]
[1] National Time Service Center, Chinese Academy of Sciences, Xi'an 710600, China; mltong@ntsc.ac.cn
[2] Key Laboratory of Time and Frequency Primary Standards, Chinese Academy of Sciences, Xi'an 710600, China
[3] University of Chinese Academy of Sciences, Beijing 100049, China
Received 2024 September 21; revised 2024 November 18; accepted 2024 December 12; published 2025 January 30

Abstract

Clock difference between the ensemble pulsar timescale (PT) and the International Atomic Time (TAI) PT-TAI derived from the International Pulsar Timing Array (IPTA) data set indicates a very similar variation trend with the Terrestrial Time TT(BIPMXXXX)-TAI but PT has larger measurement error. In this paper, we discuss the smoothing method of PT using a combined smoothing filter and compare the results with that from other filters. The clock difference sequence between PT-TAI and the first time derivative series of the TT(BIPMXXXX)-TAI can be combined by a combined smoothing filter to yield two smooth curves tied by the constraints assuring that the latter is the derivative of the former. The ensemble pulsar time IPTA2016 with respect to TAI published by G. Hobbs et al. and first time derivative series of the TT(BIPM2017)-TAI with quadratic polynomial terms removed are processed by combined smoothing filter in order to demonstrate the properties of the smoothed results. How to correctly estimate two smoothing coefficients is described and the output results of the combined smoothing filter are analyzed. The results show that the combined smoothing method efficiently removes high frequency noises of two input data series and the smoothed data of the PT-TAI combine long term fractional frequency stability of the pulsar time and frequency accuracy of the terrestrial time. Fractional frequency stability analysis indicates that both short and medium time interval stability of the smoothed PT-TAI is improved while keeping its original long term frequency stability level. The combined smoothing filter is more suitable for smoothing observational pulsar timescale data than any filter that only performs smoothing of a single pulsar time series. The smoothed pulsar time by combined smoothing filter is a pulsar atomic time combined timescale. This kind of combined timescale can also be used as terrestrial time.

Key words: methods: data analysis – time – (stars:) pulsars: general

1. Introduction

The rotation of millisecond pulsars is very stable, and within a few years, the stability of rotation of such millisecond pulsars rivals that of atomic clocks (Kaspi et al. 1994). It has been proposed that pulsars should be used to establish a new astronomical timescale, to which atomic time could be compared. Earlier attempts to develop a pulsar timescale have been made by Petit & Tavella (1996), Zhong & Yang (2007), Rodin (2008). Since the Pulsar Timing Array (PTA) project observing an ensemble of millisecond pulsars has been initiated, more than 50 millisecond pulsars are now being observed by the International Pulsar Timing Array (IPTA) project. The long-term timing observation data of the IPTA are available (Verbiest et al. 2016; Perera et al. 2019). The algorithm of constructing an ensemble pulsar timescale (PT) is developed and improved (Hobbs et al. 2012, 2020; Yang et al. 2022; Zhang et al. 2024). The ensemble pulsar time IPTA2016 published by Hobbs et al. (2020) includes two sets of results obtained using generalized least squares and a Bayesian algorithm. The algorithm of generalized least squares models clock errors (PT signal) as a set of equally spaced samples with an interpolation mechanism, and clock error model is included in the timing model and fitted out (for details see Hobbs et al. 2012, 2020). The Bayesian algorithm models the power spectrum of the signal of clock errors as a power law spectrum, when the model parameters are determined by Bayesian analysis, the waveform of clock errors is constructed by generalized Wiener filtration (see Lee et al. 2014; Hobbs et al. 2020). Both algorithms emphasize the importance of timing noise analysis and distinguish between noise and clock signal.

The difference between IPTA2016 and the International Atomic Time (TAI) established by generalized least squares algorithm (Hobbs et al. 2020) contains 37 data points with sampling interval of 182.6 days, the average error of the data points is 0.226 μs, and total time span of the data is 6574.5 days (from MJD 49400 to MJD 55974.5).

On the basis of the TAI, the Bureau International des Poids et Mesures (BIPM) further uses the primary frequency standard

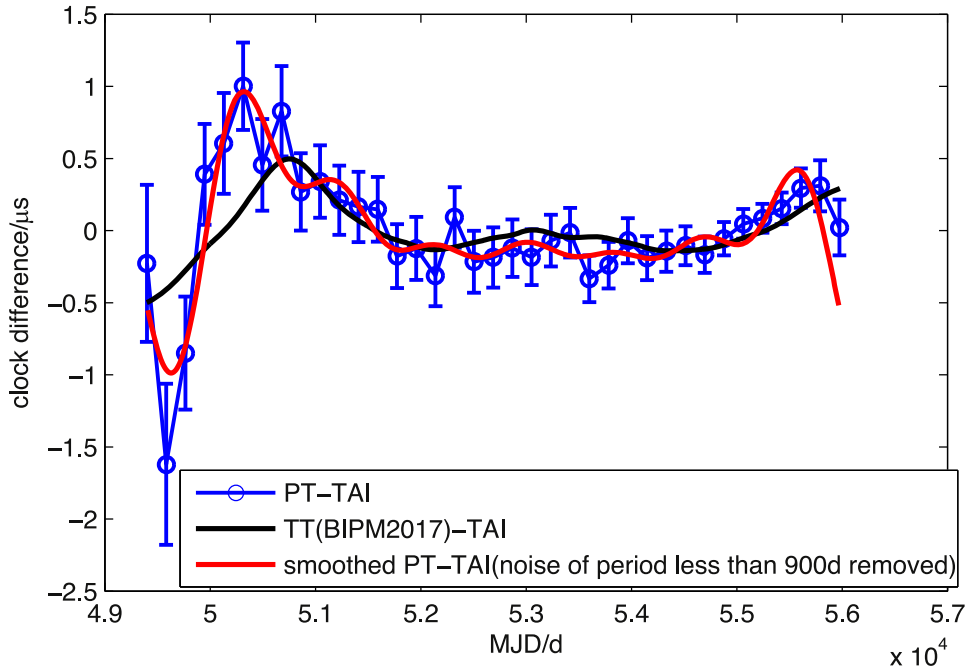

Figure 1. Comparison between the clock differences PT-TAI (blue line) and the TT(BIPM2017)-TAI (black line). The red line is smoothed cure of the PT-TAI by Fourier domain filtering.

data to obtain the comprehensive atomic time TT(BIPMxxxx). The TT(BIPMxxxx) is used as the coordinate time of the International Terrestrial Reference System (ITRS), also known as terrestrial time, and xxxx indicates the year of release. The terrestrial time is available a year later than the TAI, and updated annually. Figure 1 shows a comparison of the clock difference IPTA2016-TAI (in the following text we refer to IPTA2016 to as PT) with the difference TT(BIPM2017)-TAI obtained by anonymous ftp from the BIPM. Compared to the atomic time, the error bars of PT-TAI data points are larger, indicating large measurement error, while TT(BIPM2017)-TAI is much smoother. As shown in Figure 1, PT-TAI and TT(BIPM2017)-TAI have basically similar trends, signifying that the systematic error of the TAI is detected by PT. Several early data points of PT-TAI deviate greatly from TT (BIPM2017)-TAI mainly because the early available pulsar observations are few and the timing observation error is relatively large (Hobbs et al. 2020). At present, the published PT research results, including the results of Bayesian algorithm and Wiener filtration algorithm, can also detect systematic error of the TAI (Hobbs et al. 2012, 2020; Yang et al. 2022). It should be noted that because pulsar time does not contain linear and quadratic terms, for the data involving TT(BIPM2017)-TAI in Figure 1 and following text the linear and quadratic terms are fitted and removed.

We use σ_z to compare the fractional frequency stability of pulsar timescale with atomic timescale (Matsakis et al. 1997). Defined in terms of third-order polynomials fitted to sequences of measured time offsets, σ_z is sensitive to variations in the frequency drift rate of the clock or pulsar. Figure 2 shows the comparison of frequency stability curves for the clock difference PT-TAI with the TT(BIPM2017)-TAI. Due to the influence of measurement error, the frequency stability curve of the PT-TAI shows an approximately linearly decreasing trend with increasing time interval, and the stability of the maximum time interval is close to that of the TT(BIPM2017)-TAI. As the time series of PT extends, its long-term frequency stability has the potential for further improvement. Contrary to the PT-TAI, TT(BIPM2017)-TAI has better short-term frequency stability, but the curve gradually rises with the time interval increasing.

In order to make full use of the long-term frequency stability of the PT and improve its stability level on short- and medium-time intervals, it is necessary to study the noise removal method of PT. In the following text, PT-TAI and TT(BIPM2017)-TAI data are used as a study and analysis example of the PT noise removal method. Through analysis and comparison by applying different noise removal methods to the PT-TAI, we find that the combined smoothing method (Vondrak & Cepek 2000) produces satisfactory results. The method combines the clock difference series of PT-TAI data with the first time derivative of TT(BIPM2017) -TAI data to yield two smoothed curves such that one is smoothed PT-TAI and the other is its first time derivative. Although PT-TAI has good long-term frequency stability, the PT-TAI observation

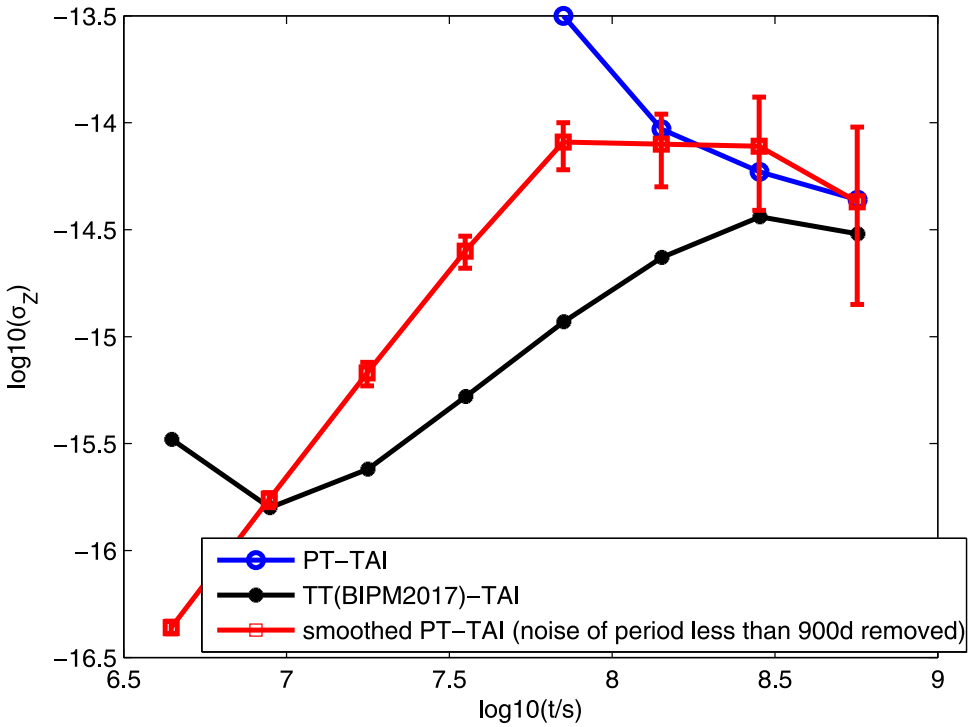

Figure 2. Comparison of fractional frequency stability σ_z curves of the TT(BIPM2017)-TAI (black line) and the clock differences PT-TAI before (blue line) and after (red line) smoothing by Fourier domain filtering.

data points are sparsely sampled and their errors are relatively large, hence it is difficult to provide information about short-term variations of clock difference by the PT-TAI. On the contrary, the TT(BIPM2017)-TAI with sampling interval 10 days has better frequency accuracy and short-term frequency stability. Therefore, the TT(BIPM2017)-TAI can provide short-term variation information on the clock difference, i.e., information on the first time derivative of the clock difference. At the same time, the long-term fractional frequency stability of the PT-TAI can constrain long-term variation of the first time derivative of TT(BIPM2017)-TAI. The function of a simple low-pass filter is to remove high frequency noise. The combined smoothing method not only can remove high frequency noise of PT-TAI, it can also combine the long-term stability of pulsar time and frequency accuracy of the terrestrial time. The smoothed PT-TAI, while maintaining its original long-term frequency stability, significantly improves its level of frequency stability at short- and medium-time intervals.

Liu et al. (2023) used a combined smoothing method, while Zhu et al. (2024) employed a wavelet analysis method to combine ensemble pulsar time and ensemble atomic time, but they did not discuss the problem of combining pulsar time and atomic frequency standards. We describe the role of frequency standards in establishing timescale in Section 4.1.

In the paper, we will focus on the usage of the combined smoothing method to combine the PT-TAI and the first time derivative of TT(BIPM2017)-TAI data sets. In Section 2, some noise removal methods of observational data, especially the combined smoothing method, are briefly described; In Section 3, the process and results of smoothing both PT-TAI and first derivative of the TT(BIPM2017)-TAI using the combined smoothing method are presented in detail; In Section 4 some application of combined timescale produced by combined smoothing filter is discussed; The final section gives the preliminary conclusion.

2. Smoothing Method of Ensemble Pulsar Timescale

In order to compare simple low-pass filtering against the combined smoothing filtering, in the following text both types of filters are introduced and their smoothed results are compared.

2.1. Fourier Domain Filtering

By a suitable filter to remove high frequency noise of the observed data, we can extract low frequency signals of interest. For example, using the Fourier domain filtering can remove the high frequency noise components of the observed data. To perform the Fourier transformation and compare the smoothed result with atomic time, we interpolated the PT-TAI linearly into a time series with 10 day spacing. Fourier transformation of the interpolated PT-TAI is performed, then the series, after

discarding the Fourier high frequency components and the signal with period longer than 900 days, is transformed to the time domain (Matsakis et al. 1997). The resulting smoothed PT-TAI after removing the high frequency noise is shown in the red line in Figure 1. The frequency stability σ_z curve in the red line of the smoothed PT-TAI is presented in Figure 2. Figure 2 clearly shows that the frequency stability of the smoothed PT-TAI for some medium-time intervals has a higher value than that for both shorter and maximum time intervals.

2.2. Combined Smoothing Method

The Vondrak smoothing method (Vondrak 1969, 1977) is popularly used in many branches of astronomy. The smoothed result of the PT-TAI using this method will be given in Section 3.

On the basis of the Vondrak smoothing method of the observational data, Vondrak & Cepek (2000) published the combined smoothing method. The method smooths two sets of observational data: In general, one with measured function values of a certain quantity whose analytic expression is unknown (Series 1) and the other with measured time derivatives of the same quantity (Series 2). Both series are measured independently or measured with different observation techniques and given at unequally spaced epochs that need not be necessarily identical, and the individual observations are given with different precision, defined by their formal uncertainties. For example, in the International Earth Rotation Service, measured polar motion and polar motion rate data are processed by the combined smoothing method; universal time UT1 obtained by VLBI observation and day length variation data series measured by GPS are combined by combined smoothing. The smoothed results of two series are defined at all data points of the two input data sets, and two sets of output series have the same number of data points. If the number of data points in two sets of input data is respectively $n1$ and $n2$, and observation epochs of the two sets of data are completely independent (no epoch overlapping data points), then the number of data points of each output data set of combined smoothing filter will be $N = n1 + n2$. Otherwise, the number of data points where the observation epoch overlaps between the two sets of input data should be subtracted. In this case, there is $N < n1 + n2$.

The basic idea of the combined smoothing method is to find the suitable weighted compromise smoothing scheme that satisfies the three different constraint conditions: smoothness of the searched curve, its fidelity to the observed function values and its fidelity to the observed first time derivatives. Let y_i, $i = 1, 2, \ldots, N$, represent the value of the ith data point on a smoothed curve of the observed function values to be searched. Supposing that the mathematical expression for the smoothness of the smoothed curve is S, the expression for the fidelity of the smoothed curve to the observed data is F, and the expression for the fidelity of the first derivative of the smoothed curve to the input first time derivative data is $\bar{F}$, all three expressions can be written in a functional form of y_i. We are looking for the smoothed y_i values as a compromise among three different conditions. The adjustment is then done by minimizing a combination of the constraints above, i.e., the expression

$$Q = S + e1 \times F + e2 \times \bar{F} = \min, \tag{1}$$

and we have

$$\frac{dQ}{dy_i} = 0. \tag{2}$$

In Equation (1), $e1 \geqslant 0$, $e2 \geqslant 0$, and these two parameters are the coefficients of smoothing chosen for the combined smoothing method. The degree of compromise among the three conditions is achieved by choosing the values of two parameters. From Equation (2) the system of N linear equations with unknowns y_i can be obtained, and the unknowns can be solved by using the known observation data (including the observed function values of the smoothed curve and its observed first derivative values). Then using the derived smoothed values y_i the smoothed values of the first derivative are calculated by formula (4–7) in Vondrak & Cepek (2000). For details on the analytical expressions for S, F and $\bar{F}$ in Equation (1) and the expressions of partial derivatives for Q in Equation (2), see Vondrak & Cepek (2000).

The two parameters $e1$ and $e2$ have respectively the dimensions [time^{-6}] and [time^{-4}]. The larger their values are, the larger weight we assign to the observed function values or their first derivatives, and the closer to the observations are the smoothed values. There is a close relation between the coefficients of smoothing and the transfer function of the combined smoothing filter (i.e., the ratio between the amplitude of the smoothed curve and the observed amplitude of a periodic function with frequency f). The transfer function T for the observed function values is analytically expressed by $e1$ and frequency f as

$$T = \frac{1}{1 + (e1)^{-1}(2\pi f)^6}. \tag{3}$$

Similarly, the transfer function $\bar{T}$ for the observed first derivatives in terms $e2$ and frequency f can be expressed as

$$\bar{T} = \frac{1}{1 + (e2)^{-1}(2\pi f)^4}. \tag{4}$$

As for choosing a pair of smoothing coefficients, if the frequency of the two sets of input data to be suppressed by the filter is known in advance, the smoothing coefficients can be calculated by Equations (3) and (4) respectively. Assuming that half of the amplitude of a high frequency period needs to be suppressed by the filter, the period is expressed as $p_{0.5}$, and its corresponding transfer function is $T = \bar{T} = 0.5$. A shorter period than $p_{0.5}$ is suppressed more strongly, and otherwise,

suppressed weakly. Then we can calculate the corresponding smoothing coefficients by using the following formulas

$$e1(p_{0.5}) = \left(\frac{2\pi}{p_{0.5}}\right)^6,\ e2(p_{0.5}) = \left(\frac{2\pi}{p_{0.5}}\right)^4. \quad (5)$$

If we want 99% of a periodic signal $p_{0.99}$ to be passed by the filter, its corresponding transfer function is $T = \bar{T} = 0.99$, then the formulas for calculating the two smoothing coefficients can be expressed as

$$e1(p_{0.99}) = 99\left(\frac{2\pi}{p_{0.99}}\right)^6,\ e2(p_{0.99}) = 99\left(\frac{2\pi}{p_{0.99}}\right)^4. \quad (6)$$

Equation (6) is especially suitable for cases where more heavy smoothing is required.

3. Data and Analysis

3.1. The Input Data for Combined Smoothing Filter

Data sequence of the difference between ensemble pulsar time IPTA2016 in Hobbs et al. (2020) and TAI (as illustrated by the blue line of Figure 1) was used. The clock difference IPTA2016-TAI is referred to as PT-TAI in the following text. The input data of clock difference series for combined smoothing filter is the PT-TAI, Including the data point sampling date MJD, clock difference values and their corresponding weights used for the filter. The error of each data point is different, and its weight is taken as the reciprocal of square of the measurement error.

Another set of input data for the filter is first time derivative (i.e., frequency difference) series derived by difference between the terrestrial timescale and TAI. TT(BIPM2017)-TAI is used for calculating first time derivative and should have approximately the same time span as the PT-TAI. Because the PT-TAI does not contain linear or quadratic terms, the first time derivative must be calculated using the TT(BIPM2017)-TAI that eliminated the linear and quadratic terms. We use the central difference method to calculate first time derivative of each data point of the TT(BIPM2017)-TAI. That is to say, the first order derivative of the middle clock difference data point is computed using the corresponding clock difference values of three adjacent data points. To calculate first derivative of the clock difference data points at the head and tail endpoints, a quadratic polynomial was fitted using the three data points located at the endpoint, and then first derivative of the endpoint is derived from the quadratic polynomial obtained by the fitting. The calculated first derivative sequence has exactly the same number of data points and sampling interval as the clock difference TT(BIPM2017)-TAI sequence, containing 659 data points, as traced by the blue line in Figure 3. Because errors of all data points in the TT(BIPM2017)-TAI clock difference sequence are similar, all data points in the first derivative sequence have equal weight. The input data of the first time derivative series for the filter include the data point sampling date MJD, first order derivative values and their weights.

3.2. Estimation of Smoothing Coefficients

There are two possibilities for choosing the smoothing coefficients $e1$ and $e2$, both requiring at least approximate a priori knowledge of the observed process of the input data sets; we should have a realistic estimation of either the precision of the measurement, or the shortest period contained in the signal (Vondrak & Cepek 2000). In our case, the measurement error of the PT-TAI data points is much larger than that of the TT(BIPM2017)-TAI data points. If the smoothing coefficients of the combined smoothing method filter are estimated according to the measurement errors of the two sets of input data, the resulting $e1$ should be too small and $e2$ should be too large, therefore the PT-TAI weight is too small, and the weight of the first derivative of TT(BIPM2017)-TAI is too large. As a result, the two sets of smoothed data produced by the filter are very close to the TT(BIPM2017)-TAI and its first time derivative respectively.

If the shortest period contained in the signal of the data is known, it is recommended to choose the values $e1$ and $e2$ as given by Equations (5) for $p_{0.5}$ lying approximately between one third and one half of the shortest known period contained in the signal. Alternatively, it is also possible to calculate $e1$ and $e2$ from Equations (6), in which we put $p_{0.99}$ equal to the shortest known period of the signal. Any values of $e1$ and $e2$ lying in the vicinity of these yield approximately the same acceptable results (Vondrak & Cepek 2000).

We assumed that the shortest period of the signal contained in the data is about 3 yr and use $p_{0.99} = 3$ yr to calculate the coefficients of smoothing $e1$ and $e2$. The derived solution of the filter indicates that the smoothed first time derivative sequence significantly deviates from its input data. The large deviation is caused by the noise of PT-TAI which is not sufficiently smoothed. Then we decided to do grid searches to find the shortest period of the signal $p_{0.99}$ in the input data sets that is best suited for calculating a pair of smoothing coefficients.

Let $p_{0.99} = 0.1, 0.2, \ldots, 12$ yr (12 yr is greater than half of the PT-TAI time span), and substituting $p_{0.99}$ into formula (6), we obtain their corresponding $e1$ and $e2$ value sequences. Using $e1$ and $e2$ sequence values, the combined smoothing method filter smooths out the PT-TAI series and first derivative series of the TT(BIPM2017)-TAI and calculates standard deviation of the weighted average of the respective residuals (differences between the filter input values and the corresponding smoothed values of the output) for both PT-TAI series and first derivative series of the TT(BIPM2017)-TAI. Figure 4 shows the relationship curve between $p_{0.99}$ used to calculate smoothing coefficients and the corresponding standard deviation. The upper subplot is for $e1$ and lower is for $e2$ in Figure 4.

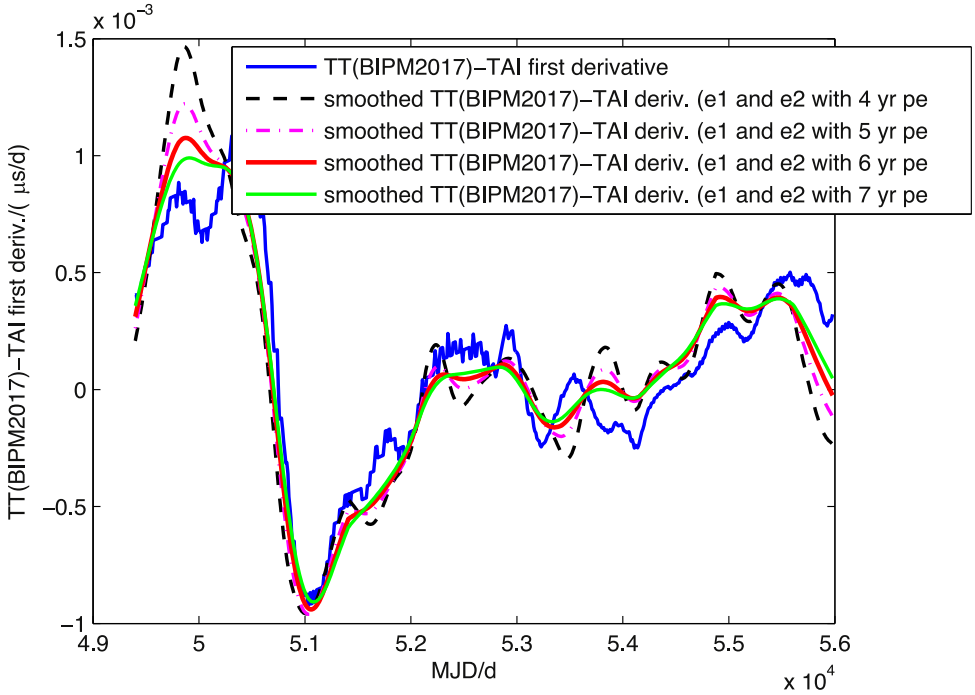

Figure 3. First time derivative of the TT(BIPM2017)-TAI and its smoothed curves derived by the combined smoothing method using four pairs of smoothing coefficients $e1$ and $e2$ respectively.

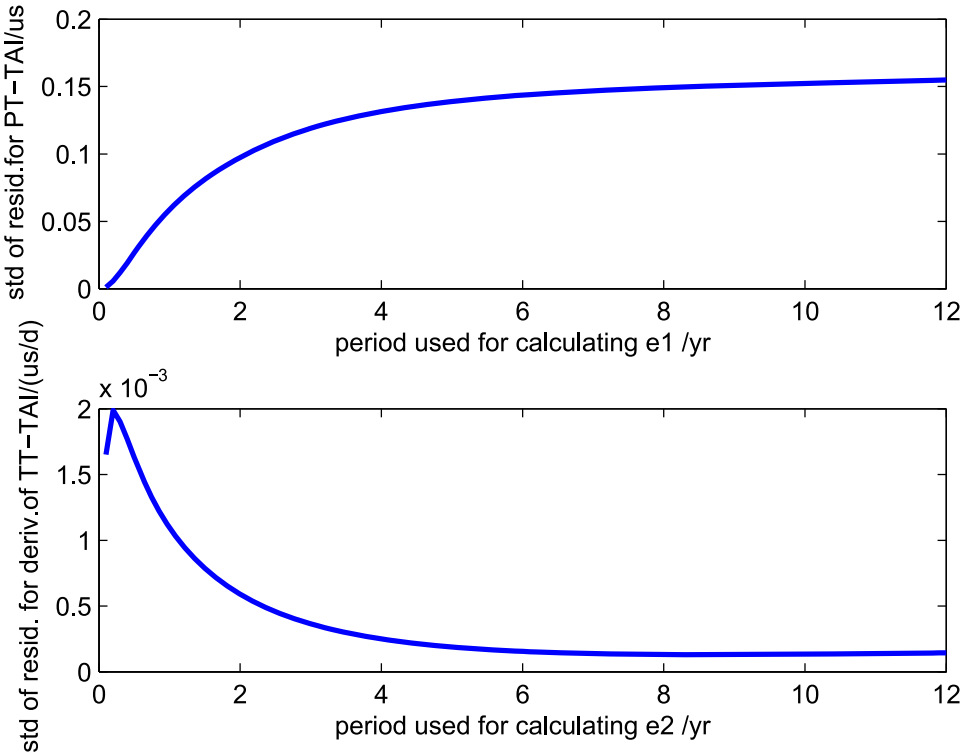

Figure 4. Relationship curve between residual standard deviation and period $P_{0.99}$ used to calculate $e1$ (upper) and $e2$ (lower) for combined smoothing filter.

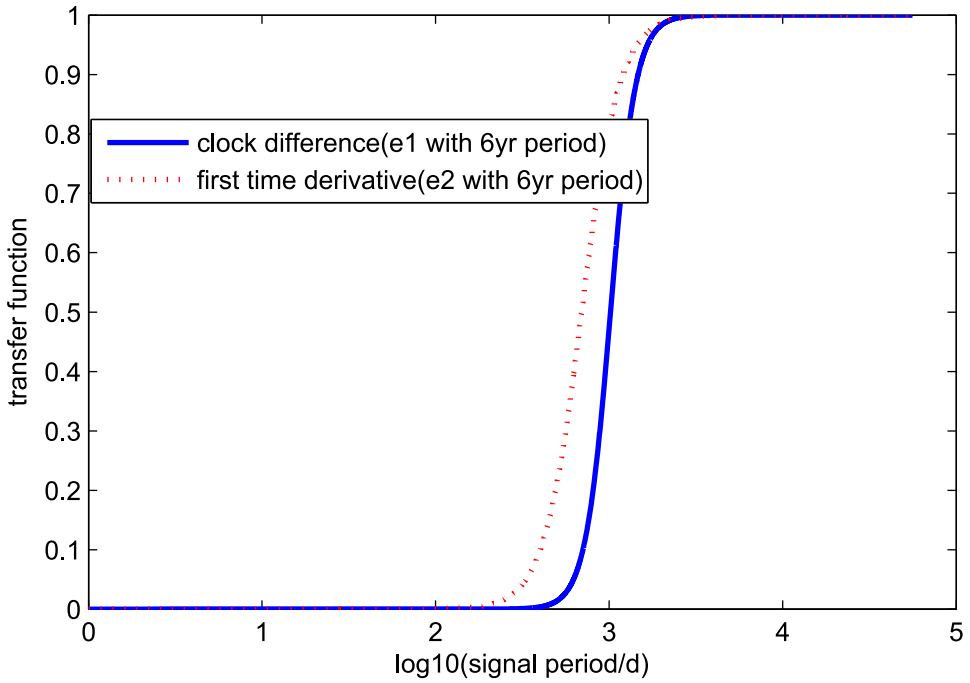

Figure 5. Transfer functions for the PT-TAI and first derivative of the TT(BIPM2017)-TAI (using 6 yr period to calculate $e1$ and $e2$).

The smaller the period value used for calculating smoothing coefficient is, the larger is the value of smoothing coefficient derived. The larger the value of smoothing coefficient used is, the weaker is the smoothed degree of the corresponding input data sequence. The upper subplot in Figure 4 shows that at $p_{0.99} < 6$ yr the residual standard deviation increases as the period used to calculate $e1$ increases, and at $p_{0.99} \geqslant 6$ yr the curve of residual standard deviation gradually levels off for the PT-TAI. On the contrary, in the lower subplot, at $p_{0.99} < 6$ yr, excluding the first data point, the residual standard deviation decreases with increasing period $p_{0.99}$ and at $p_{0.99} \geqslant 6$ yr the curve of residual standard deviation gradually levels off for first derivative data of the TT(BIPM2017)-TAI. This phenomenon is caused by the incompatibility of the errors of two sets of data (large error of PT-TAI versus small error of first derivative of TT(BIPM2017)-TAI)). The larger measurement errors of PT-TAI lead to a large fluctuation in their sampled data points. In the weak smoothing case, the smoothed curve of first derivative deviates greatly from its true value due to the PT-TAI error, so that the standard deviation of the first derivative residuals is larger. As the period value used for calculating smoothing coefficients increases, the PT-TAI is progressively moderately smoothed, bringing the smoothed curve of the first derivative gradually closer to the correct one. An illustration of the smoothed first derivative curves of combining two input data sets using $e1$ and $e2$ with four different $p_{0.99}$ values is given in Figure 3. We see that in Figure 3 the first derivative smoothed curve derived using smoothing coefficients with 4 yr period clearly shows some deviation because of insufficiently smoothed noise of the PT-TAI. When the $p_{0.99}$ value used gets larger, this kind of deviation is gradually suppressed and removed.

According to Figure 3, it is recommended to carry out combined smoothing for the PT-TAI and first derivative of the TT(BIPM2017)-TAI using the calculated smoothing coefficients $e1$ and $e2$ with $p_{0.99} = 6$ yr. Choosing the smoothing coefficients with $p_{0.99} = 6$ yr, the high frequency noise of PT-TAI can be sufficiently smoothed and the interesting signal is not suppressed. For the smoothing coefficients $e1$ and $e2$ calculated with 6 yr period, the corresponding transfer function curves of the filter are shown in Figure 5 where the blue solid and red dotted lines are respectively the transfer functions of the PT-TAI clock difference and first derivative of the TT(BIPM2017)-TAI. In Figure 5 the abscissa is the logarithm of the signal period. As can be seen from Figure 5, the curves of the transfer function of the two sets of data are similar, and the first derivative transfer function is slightly shifted more toward the short period end than the clock difference transfer function. The transfer functions shown in Figure 5 yield better smoothed results for both sets of data simultaneously. If changing the value of $e1$ to shift the blue line to nearly overlap the red dotted line, or changing the value of $e2$ to shift the red dotted line to nearly overlap the blue line, in these two cases the smoothed curve of the first derivative is obviously affected, fluctuation of the curve becomes larger, and the residual standard deviation becomes larger, whereas standard deviation

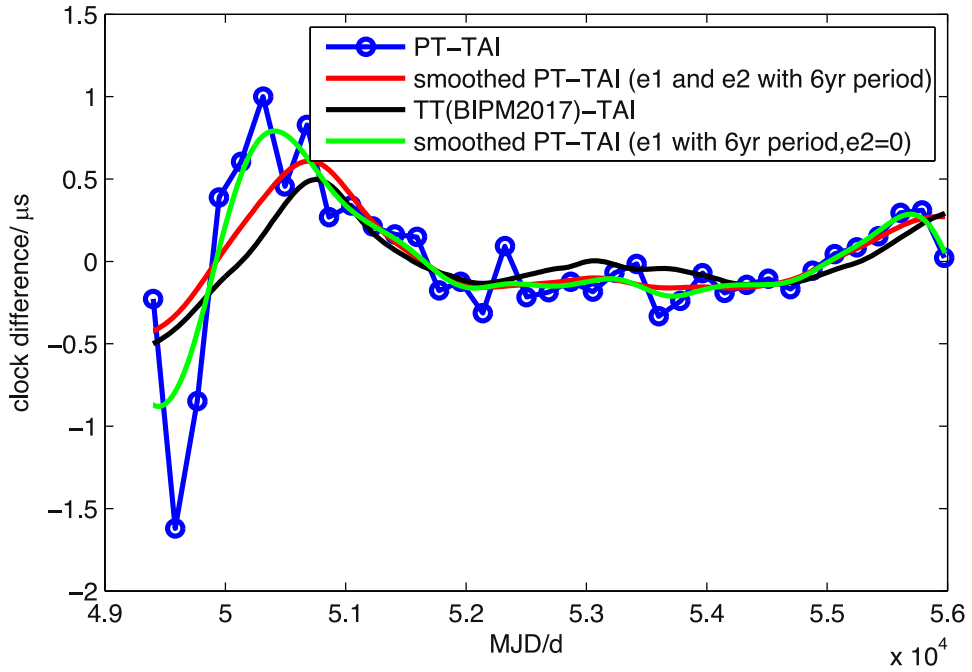

Figure 6. Comparison of the PT-TAI before (blue line) and after (red line) combined smoothing using $e1$ and $e2$ with 6 yr period. The TT(BIPM2017)-TAI is displayed in a black line. The green line is the smoothed PT-TAI using $e1$ with 6 yr period and $e2 = 0$. The behavior of the green curve is similar to that of the smoothed PT-TAI by Fourier domain filtering in Figure 1.

of the clock difference curve becomes smaller. In order to balance smoothed results for both clock difference and first derivative, the two smoothing coefficients of the filter should be calculated using the same suitable $p_{0.99}$ value. We finally adopt the smoothed results for the two sets of data in the case with $p_{0.99} = 6$ yr.

3.3. Analysis of Smoothed Results

The smoothing coefficients $e1$ and $e2$ with $p_{0.99} = 6$ yr are used for the combined smoothing filter to smooth the PT-TAI and first derivative series of the TT(BIPM2017)-TAI. Since observation epochs of the two sets of data do not overlap, the number of data points for each one of the two sets of data after smoothing are equal to the sum of the data points of the two sets of original data. Figure 6 shows the smoothed PT-TAI curve (red line). To facilitate the comparison, Figure 6 again presents the original PT-TAI data (blue line) and the terrestrial time TT(BIPM2017)-TAI (black line). From Figure 6 we see that the smoothed PT-TAI curve is more similar to that representing TT(BIPM2017)-TAI than the original one. Figure 3 shows the TT(BIPM2017)-TAI first derivative curve (red line) after the smoothing and the original TT(BIPM2017)-TAI first derivative (blue line). Figure 7 shows the residuals of the two sets of data and their corresponding histograms. The upper left subplot is the PT-TAI residuals. The subplot shows that the large residuals appear in the early PT-TAI data where the residual absolute value, especially for the second data point, is greater than 1 μs. After that, the absolute value of residual of each data point gradually decreases, indicating that the accuracy of pulsar timing is constantly improving. The standard deviation of residuals of the PT-TAI after filter smoothing is 0.144 μs. Although the mean measurement error of the original PT-TAI data is 0.226 μs, the weighted mean of the measurement error is 0.164 μs which is close to the standard deviation of residuals of the PT-TAI after smoothing. The upper right subplot is the residual curve of the TT(BIPM2017)-TAI first derivative after filter smoothing, and the standard deviation of the first derivative residuals is 0.000155 μs/d. To further investigate the residual distribution of the two sets of smoothed data, we present the histograms of the respective residuals in Figure 7. In Figure 7, the lower left subplot is the histogram of distribution of PT-TAI residuals, and the lower right subplot is the histogram of distribution of TT(BIPM2017)-TAI first derivative residuals. Both histograms are very close to a Gaussian distribution, demonstrating that the smoothed results by computing $e1$ and $e2$ with $p_{0.99} = 6$ yr efficiently eliminate the high frequency noise in the two sets of data, correctly extracting the signal of PT-TAI. The first time derivative of the smoothed PT-TAI is equal to the smoothed first time derivative of TT(BIPM2017)-TAI, in other words, both smoothed PT-TAI and TT(BIPM2017)-TAI have the same frequency difference.

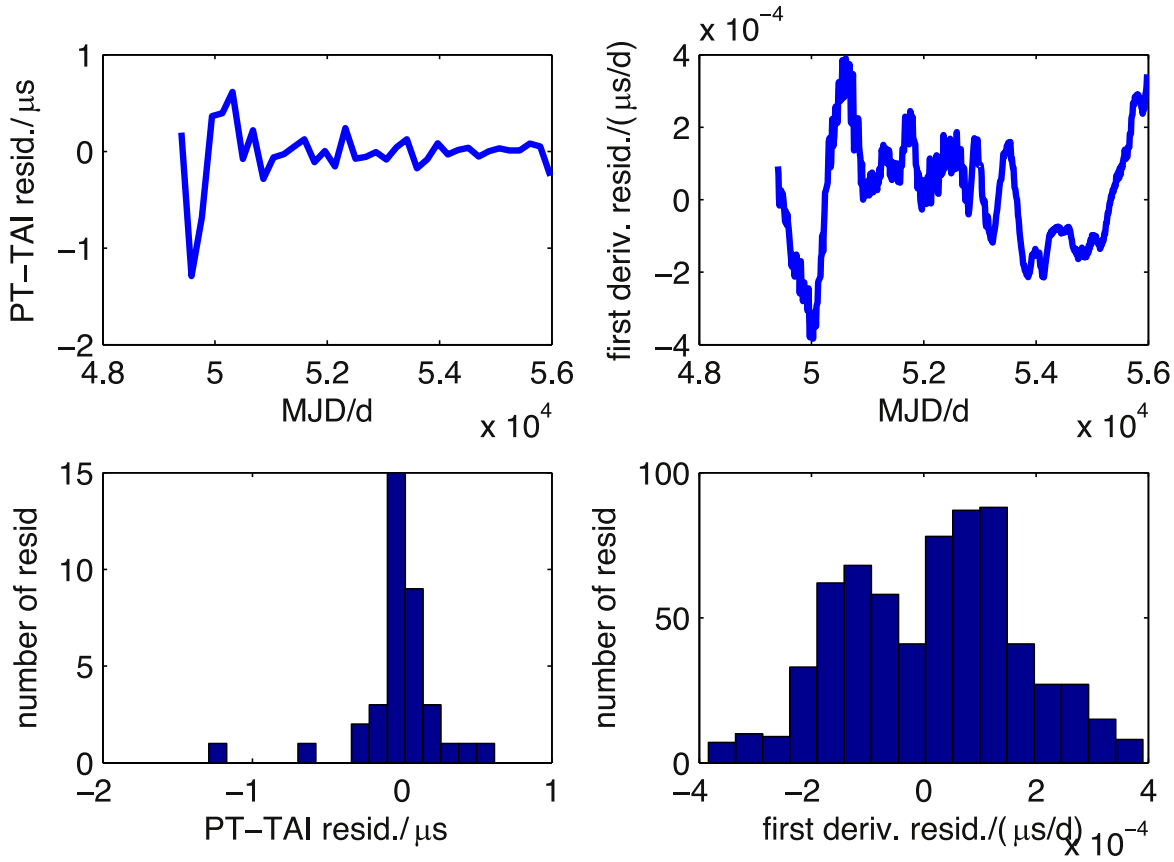

Figure 7. Residuals of PT-TAI series (upper left) and distribution histogram (lower left); Residuals of first derivative series of TT(BIPM2017)-TAI (upper right) and distribution histogram (lower right). The coefficients $e1$ and $e2$ with 6 yr period are used for the combined smoothing filter.

We also calculated the smoothed curve of PT-TAI using coefficient $e1$ with $p_{0.99} = 6$ yr and setting $e2 = 0$. In this case, the problem reduces to original smoothing (Vondrak 1969, 1977), and the first derivative of the TT(BIPM2017)-TAI is simply ignored. The smoothed curve of PT-TAI obtained in this way is shown with the green line in Figure 6.

We analyze fractional frequency stability σ_z of the PT-TAI before and after combined smoothing and compare it with that of the TT(BIPM2017)-TAI. Figure 8 shows the σ_z curve (red line) of the PT-TAI after smoothing using $e1$ and $e2$ with $p_{0.99} = 6$ yr. The σ_z curve of the smoothed PT-TAI using $e1$ with 6 yr period and $e2 = 0$ is also shown in the green line. For easy comparison, in Figure 8, σ_z curves of the original data, PT-TAI (blue line), and the TT(BIPM2017)-TAI (black line) are presented again. As can be seen from Figure 8, the σ_z curve of the smoothed result by the filter using the calculated $e1$ and $e2$ with $p_{0.99} = 6$ yr shown with the red line improves both the short- and medium-time interval frequency stability levels compared to the blue line. Although the green line significantly improves the PT-TAI short-term frequency stability, its σ_z for some medium-time intervals indicates a higher value than that of the red line. The behavior of the green line is similar to that of the smoothed result by Fourier domain filtering in Figure 2. Figure 8 indicates that the smoothed PT-TAI by combined smoothing filter has the best short time stability and its long-term stability is comparable with that of TT(BIPM2017)-TAI.

We can understand the result from another point of view. Figure 9 depicts the power spectral density of both TT(BIPM2017)-TAI and smoothed PT-TAI obtained using $e1$ and $e2$ with $p_{0.99} = 6$ yr. As Figure 9 shows, both curves indicate the significant low frequency signal, but the low frequency signal of the smoothed PT-TAI is stronger than that of TT(BIPM2017)-TAI. As the frequency increases, the smoothed PT-TAI signal becomes weaker than TT(BIPM2017)-TAI, so that in the high frequency band, the power spectral curve is completely below that of TT(BIPM2017)-TAI. This also signifies that TT(BIPM2017)-TAI still contains some high frequency noise, which is indirectly demonstrated by the high frequency noise of the first time derivative curve (see Figure 3). Incidentally, the smoothed PT-TAI power spectral curve (red line) as shown in Figure 9 is different from the power spectrum of the PT-TAI

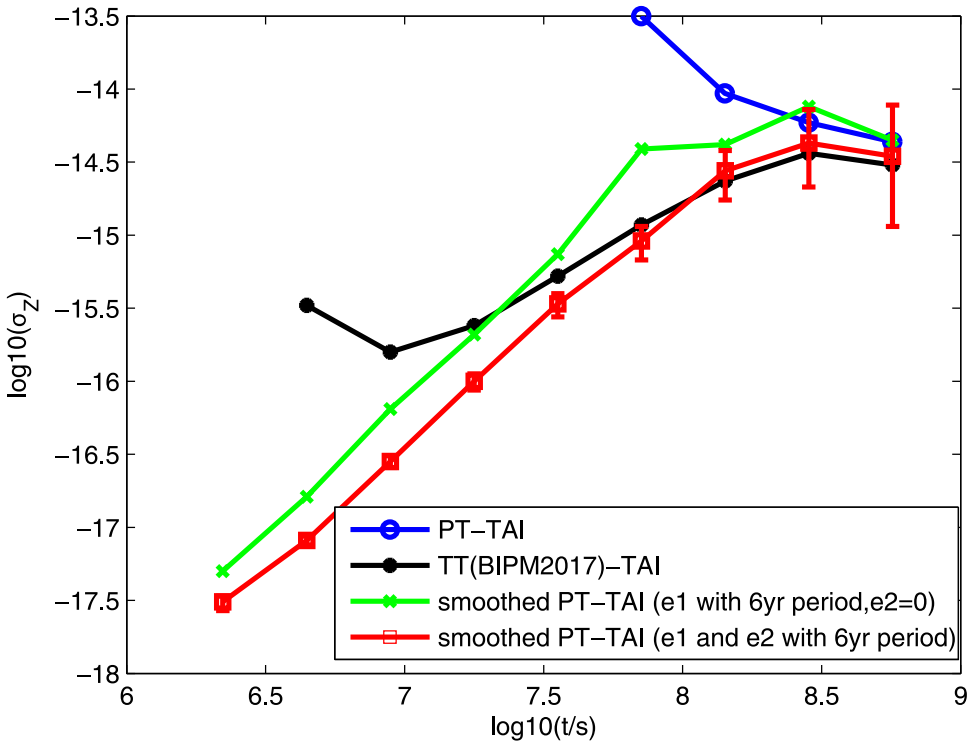

Figure 8. σ_z curves of timescales with respect to TAI.

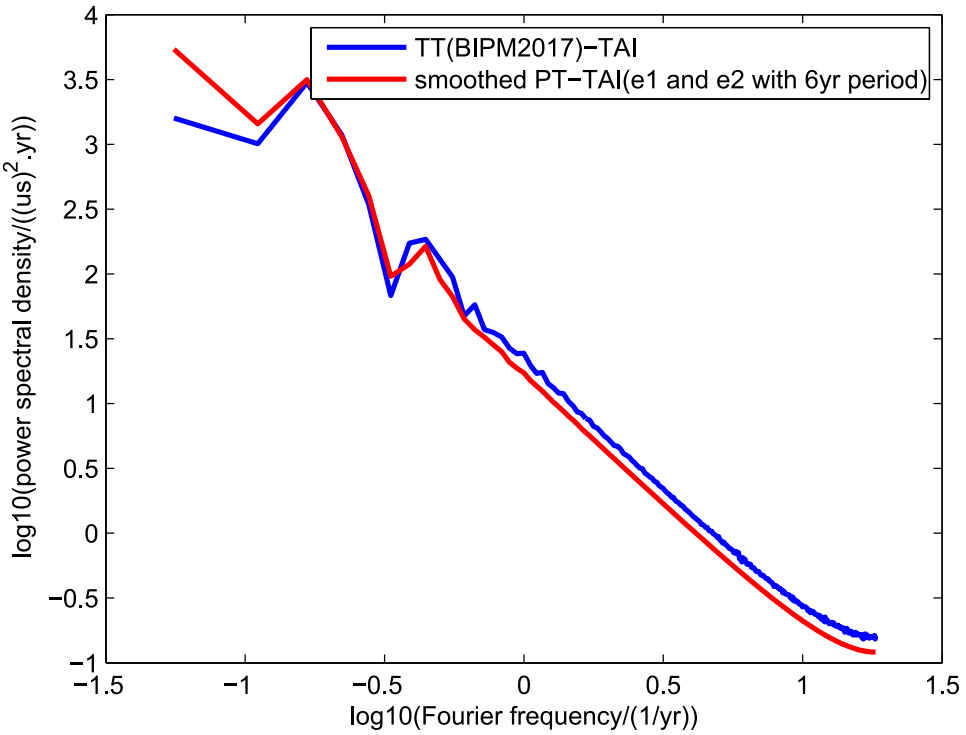

Figure 9. Power spectral density curves of the smoothed PT-TAI (red line) and of TT(BIPM2017)-TAI (blue line).

smoothed by Fourier domain filtering as shown in the red line of Figure 1. The spectral intensity in the high frequency band of the former gradually decreases with increasing frequency, whereas the high frequency band spectral intensity of the latter is mutated to 0 from the cutoff frequency.

4. Application for Pulsar Atomic Clock Combined Timescale

4.1. Using as Terrestrial Time

The ideal timescale for the coordinate time of ITRS should have good frequency stability and frequency accuracy. The accuracy means the scale interval (unit) is based on SI second. TAI gets its stability from some 400 atomic clocks kept in some 80 laboratories worldwide and its accuracy from a small number of primary frequency standards (PFS) developed by a few metrology laboratories through frequency steering correction. Because TAI is computed in quasi-real-time every month and has operational constraints (e.g., no re-computation on a given time interval even if new data become available), it does not provide an optimal realization of terrestrial time. The BIPM therefore computes another realization TT(BIPMxxxx) in post-processing. TT(BIPMxxxx) has better stability and accuracy than TAI.

Although pulsar time PT derived from PTA data set exhibits good long-term stability, its measurement error is much larger than atomic time and frequency accuracy is not guaranteed to conform with an SI second. Figure 6 shows that the green curve (smoothed PT-TAI using $e1$ with 6 yr period and $e2 = 0$) is very different from the red curve (smoothed PT-TAI by combined smoothing using $e1$ and $e2$ with 6 yr period), correspondingly their first derivative (frequency difference) curves should be very different, i.e., the unit (second) of the original PT is very different from an SI second. The smoothed PT by combined smoothing filter combines long-term stability of PT and accuracy of TT(BIPMxxxx) and removes high frequency noise of original PT, so in essence smoothed PT is a combined timescale with TT(BIPMxxxx); hereafter we refer it to as combined pulsar atomic time (CPA). Because both frequency stability and accuracy of CPA are comparable to those of TT(BIPMxxxx), CPA can also be taken as terrestrial time. In this work TT(BIPM2017) is used as the frequency standard to compute frequency difference of TT(BIPM2017)-TAI used for combined smoothing filter. In the future, PFS instead of TT(BIPMxxxx) should be utilized to compute the frequency difference of clock difference between PFS and TAI. In this way, we will combine long-term stability of the original PT with frequency accuracy of PFS. Producing CPA using PT and PFS has an advantage compared to TT(BIPMxxxx). In the future, ensemble pulsar time with respect to TAI may be produced in quasi-real-time every month, using PFS as the frequency standard to realize SI second, then CPA timescale can be derived utilizing a combined smoothing filter in quasi-real-time every month, whereas TT(BIPMxxxx) will be available a year later. Since both PT and PFS will continue to develop, in the future, CPA may be further improved.

4.2. Steering Atomic Clock

A quasi-real-time timescale with high quality can be used as a reference standard for steering some clock. For example, a hydrogen maser shows very good short time (within a month) frequency stability, but its stability gradually decreases with increased time interval, though steering a hydrogen maser to a timescale with a high quality hydrogen maser can supply, in real-time to a user, a time signal with high stability and accuracy in a needed long time interval. CPA can be used as a reference standard to steer a clock.

As an example of a clock steering experiment, we choose the local atomic time kept by the United States Naval Observatory, TA(USNO), as a timescale to be steered. Like a hydrogen maser, TA(USNO) has good short-term frequency stability, but its long-term stability gradually becomes worse. Data for clock difference TAI-TA(USNO) are taken from the BIPM website. To be consistent with time span of the TAI-TA(USNO) available, a data series after MJD 50678 for the CPA-TAI shown in Figure 6 (red curve) is used. From TAI-TA(USNO) and CPA-TAI data sets, we derived clock difference series CPA-TA(USNO) with regular sampling.

We assume clock difference, frequency difference and frequency drift for TA(USNO) with respect to reference standard CPA at moment k respectively to be a_k,b_k and c_k. If a_k, b_k and c_k are known, the clock difference a_{k+1} at moment $k + 1$ can be derived by

$$a_{k+1} = a_k + b_k \Delta t + \frac{1}{2} c_k \Delta t^2 + n_{k+1}, \tag{7}$$

where Δt is the sampling interval and n_{k+1} is the noise term. We use a Kalman filter (Kalman 1960, Brown & Hwang 1983, Pìriz et al. 2019) to determine a_k, b_k and c_k. For the Kalman filter, the input data series is CPA-TA(USNO), and the output is a_k, b_k and c_k for each step of the filter. When a_k, b_k and c_k are determined by the filter then clock difference CPA-TA(USNO) is corrected according to Equation (7). In this way TA(USNO) is steered to the reference standard CPA. The differences between CPA and steered TA(USNO), i.e., residuals of steering TA(USNO) to CPA, are shown in panel (b) of Figure 10. For comparison, TT(BIPM2017)-TA(USNO) is processed by the Kalman filter in the same way as CPA-TA(USNO), and residuals after steering TA(USNO) to TT(BIPM2017) are displayed in panel (c) of Figure 10. In order to steer TA(USNO) to the not smoothed original PT with sparse sampling we linearly interpolate PT-TAI data and then get the PT-TA(USNO) series with the same sampling as the CPA-TA(USNO). The residuals after steering TA(USNO) to raw PT are given in panel (a) of Figure 10. The residuals in three subplots are the results after the Kalman filter

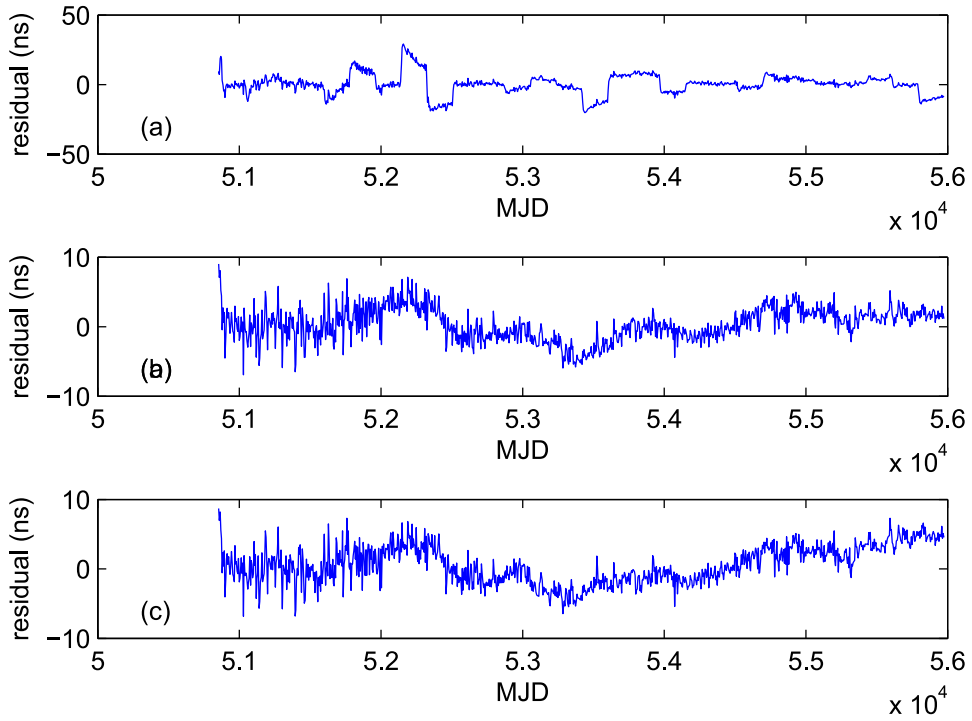

Figure 10. Residuals after steering TA(USNO) to raw PT (panel (a)), CPA (panel (b)) and TT(BIPM2017) (panel (c)).

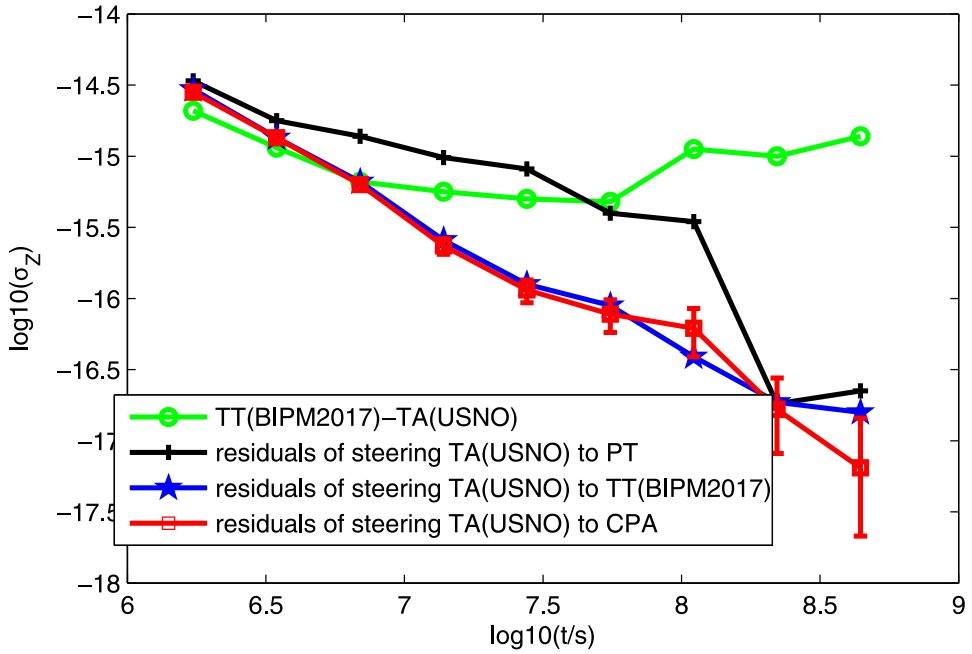

Figure 11. σ_z curves of residuals after steering TA(USNO) to different reference standards. Black, blue and red curves are for residuals of steering TA(USNO) respectively to raw PT, TT(BIPM2017) and CPA data. For comparison, the σ_z curve of TT(BIPM2017)-TA(USNO) is shown as a green line.

converged. We see that residuals of panel (b) and (c) show similar behavior with standard deviations 2.4 ns and 2.7 ns respectively. Dispersion of the residuals in panel (a) is obviously larger than both (b) and (c), because reference standard PT has large measurement error. The standard deviation of the residuals in panel (a) is 7.4 ns.

In Figure 11 we compare frequency stability curves for the residuals after steering TA(USNO) to the raw PT (black line),

TT(BIPM2017) (blue line) and CPA (red line). In Figure 11, the stability curve for TT(BIPM2017)-TA(USNO) series is also shown as a green line. Although the green line indicates better short-term stability, its long-term stability becomes worse. After frequency steering, both blue and red curves obviously improved medium and long-term frequency stability compared with the green curve. The black curve shows worse frequency stability than both blue and red curves at any time interval. The results of the frequency steering experiment also demonstrate that the property of timescale CPA is comparable with TT(BIPMxxxx), and both are better than the original PT for application.

5. Conclusion

Usually, developed ensemble pulsar time PT raw data possess sparser data points with larger error than the atomic timescale. Through correctly choosing two smoothing coefficients of a combined smoothing filter, the high frequency noise contained in both the original clock difference of PT-TAI and first derivative of TT(BIPM2017)-TAI can be efficiently removed by the filter. Data points of the PT-TAI smoothed by the filter are denser than the original data and smoothed PT-TAI takes on advantages of both long-term frequency stability from PT and frequency accuracy from the terrestrial timescale.

The smoothed PT-TAI series by combined smoothing filter can improve short and medium-time interval stability when keeping its original long-term frequency stability. Any smoothing filter that only smooths single PT-TAI data can improve short-term stability but cannot improve stability level of medium-time intervals of the smoothed curve as the combined smoothing filter does.

The primary frequency standards are used to realize SI second on which the timescale should be based. The frequency accuracy of the terrestrial timescale is determined by primary frequency standards (Guinot 1988). In the future, we can produce combined smoothing using PT-TAI raw data series and frequency difference series of the primary frequency standards with respect to TAI instead of TT(BIPMxxxx)-TAI. Here the frequency difference of primary frequency standards with respect to TAI refers to the first derivative of the corresponding clock difference from which quadratic polynomial terms are removed. By the combined smoothing filter we produce a combined timescale CPA which takes on long-term stability of PT and accuracy of primary frequency standards. The properties of stability and accuracy for CPA are comparable with those for the terrestrial time TT(BIPMxxxx). CPA can also be used as terrestrial time.

Acknowledgments

This work is supported by the Strategic Priority Research Program of Chinese Academy of Sciences (grant No. XDA0350502), the National SKA Program of China (grant No. 2020SKA0120103) and the National Natural Science Foundation of China (NSFC, Grant Nos. U1831130 and 11973046).

References

Brown, R., & Hwang, P. 1983, Introduction to Random Signals and Applied Kalman Filtering (New York: Wiley)
Guinot, B. 1988, A&A, 192, 370
Hobbs, G., Coles, W., Manchester, R. N., et al. 2012, MNRAS, 427, 2780
Hobbs, G., Guo, L., Caballero, R. N., et al. 2020, MNRAS, 491, 5951
Kalman, R. E. 1960, Journal of Basic Engineering, 82, 35
Kaspi, V. M., Taylor, J. H., & Ryba, M. F. 1994, ApJ, 428, 713
Lee, K. J., Bassa, C. G., & Janssen, G. H. 2014, MNRAS, 441, 2831
Liu, Y., Xu, B., Zheng, Z. H., et al. 2023, MNRAS, 521, 2553
Matsakis, D. N., Taylor, J. H., & Eubanks, T. M. 1997, A&A, 326, 924
Petit, G., & Tavella, P. 1996, A&A, 308, 290
Perera, B. B. P., Decesar, M. E., Demorest, P. B., et al. 2019, MNRAS, 490, 4666
Pìriz, R., Garbin, E., Keith, M., et al. 2019, in Proc. of the 50th Annual Precise Time and Time Interval Systems and Applications Meeting, 191
Rodin, A. E. 2008, MNRAS, 387, 1583
Verbiest, J. P. W., Lentati, L., Hobbs, G., et al. 2016, MNRAS, 458, 1267
Vondrak, J. 1969, BAICz, 20, 349
Vondrak, J. 1977, BAICz, 28, 84
Vondrak, J., & Cepek, A. 2000, A&AS, 147, 347
Yang, T. G., Tong, M. L., & Gao, Y. P. 2022, RAA, 22, 105012
Zhang, Z. H., Tong, M. L., & Yang, T. G. 2024, ApJ, 962, 2
Zhong, C. X., & Yang, T. G. 2007, AcPSn, 10, 6157, in Chinese
Zhu, X. Z., Zhang, Z. H., Zhao, C. S., et al. 2024, MNRAS, 529, 1082